UROGENITAL

Differentiating between malignant and benign renal tumors: do IVIM and diffusion kurtosis imaging perform better than DWI?

Yuqin Ding[1] · Qinxuan Tan[1] · Wei Mao[1] · Chenchen Dai[1] · Xiaoyi Hu[2] · Jun Hou[3] · Mengsu Zeng[1] · Jianjun Zhou[1]

Abstract

Objective To quantitatively compare the diagnostic values of conventional diffusion-weighted imaging (DWI), intravoxel incoherent motion (IVIM), and diffusion kurtosis imaging (DKI) in differentiating between malignant and benign renal tumors.

Methods Multiple b value DWIs and DKIs were performed in 180 patients with renal tumors, which were divided into clear cell renal cell carcinoma (ccRCC), non-ccRCC, and benign renal tumor group. The apparent diffusion coefficient (ADC), true diffusivity (D), pseudo-diffusion coefficient (D^*), perfusion fraction (f), mean kurtosis (MK), and mean diffusivity (MD) maps were calculated. The diagnostic efficacy of various diffusion parameters for predicting malignant renal tumors was compared.

Results The ADC, D, and MD values of ccRCCs were higher, while D^*, f, and MK values were lower than those of benign renal tumors (all $p < 0.025$). The D^* and f values of non-ccRCCs were lower than those of benign renal tumors ($p = 0.002$ and $p < 0.001$, respectively). The difference of ADC, D, MD, and MK values between non-ccRCCs and benign renal tumors was not statistically significant ($p > 0.05$). The ADC, D, MD, and f values of ccRCCs were higher, while MK values were lower than those of non-ccRCCs (all $p < 0.001$). The AUC values of ADC, D, D^*, f, MK, and MD were 0.849, 0.891, 0.708, 0.656, 0.862, and 0.838 for differentiating ccRCCs from benign renal tumors, respectively. The AUC values of D^* and f were 0.772 and 0.866 for discrimination between non-ccRCCs and benign renal tumors, respectively.

Conclusion IVIM parameters are the best, while DWI and DKI parameters have similar performance in differentiating malignant and benign renal tumors.

Key Points

• *The D value is the best parameter for differentiating ccRCC from benign renal tumors.*
• *The f value is the best parameter for differentiating non-ccRCC from benign renal tumors.*
• *Conventional DWI and DKI have similar performance in differentiating malignant and benign renal tumors.*

Keywords Renal neoplasms · Diffusion-weighted MRI · Intravoxel incoherent motion · Diffusion kurtosis imaging · Differential diagnosis

Jianjun Zhou and Mengsu Zeng have the same contribution to the design and guidance of this manuscript. As a result, they are listed as co-corresponding authors of this article.

✉ Mengsu Zeng
zeng.mengsu@zs-hospital.sh.cn

✉ Jianjun Zhou
zhoujianjunzs@126.com

[1] Department of Radiology, Zhongshan Hospital, Fudan University; Shanghai Institute of Medical Imaging, 180 Fenglin Road, Shanghai 200032, People's Republic of China

[2] Department of Urology, Zhongshan Hospital, Fudan University, Shanghai 200032, People's Republic of China

[3] Department of Pathology, Zhongshan Hospital, Fudan University, Shanghai 200032, People's Republic of China

Abbreviations

ADC	Apparent diffusion coefficient
AUC	Areas under the curves
ccRCC	Clear cell renal cell carcinoma
CI	Confidence interval
D	True diffusivity
$D*$	Pseudo-diffusion coefficient
DKI	Diffusion kurtosis imaging
DWI	Diffusion-weighted imaging
f	Perfusion fraction
ICC	Intraclass correlation coefficient
IVIM	Intravoxel incoherent motion
MD	Mean diffusivity
MK	Mean kurtosis
non-ccRCC	Non-clear cell renal cell carcinoma
ROC	Receiver operating characteristic
ROI	Region of interest
SPIR	Spectral presaturation inversion recovery
TE	Echo time
TR	Repetition time

Introduction

The incidence of incidentally discovered localized renal masses has risen partly due to increased utilization of ultrasound and cross-sectional imaging [1]. Benign lesions are found at partial or total nephrectomy in up to 11% to 17.9% of cases misdiagnosed as renal cancer on preoperative imaging according to the surgical literature [2–5]. In light of the potential for iatrogenic chronic kidney disease, partial nephrectomy rather than radical nephrectomy is recommended for managing localized renal masses where feasible [6]. Recently, active surveillance has emerged as an initial management option to elderly and comorbid patients with incidentally detected small renal masses [7]. Differences in prognosis and evolving treatment paradigms based on tumor aggressiveness emphasize the need for noninvasive tools to accurately differentiate benign from malignant renal tumors.

Contrast-enhanced computed tomography (CT) and conventional magnetic resonance imaging (MRI) are routinely used in the evaluation of renal lesions; however, they still have some limitations such as exposure to ionizing radiation and potential risk of renal function impairment. Diffusion-weighted imaging (DWI), free of ionizing radiation and extraneous contrast material, could obtain information about the microscopic motion of water protons, which was indicative of changes at the cellular level [8]. DWI has been widely used to differentiate benign from malignant renal masses, grading and subtyping of RCCs [9, 10]. However, there is always concern that the apparent diffusion coefficient (ADC) obtained from conventional monoexponential DWI could not accurately reflect the real diffusivity, because of the influence of microcirculation [11, 12]. Some previous researchers have suggested that intravoxel incoherent motion (IVIM) and diffusion kurtosis imaging (DKI) might provide more accurate information about water diffusion [13, 14]. The biexponential IVIM model, proposed by Le Bihan et al [13], expresses the diffusion-weighted signal as the sum of a pure diffusion fraction and a perfusion-dominated "pseudo-diffusion" fraction. DKI is a non-Gaussian diffusion-weighted model first described by Jensen et al [15] in 2005, which is believed to better reflect the microstructural complexity of biologic tissue. Since DWI with different models and DKI may demonstrate different aspects of tissue properties, it should be valuable to explore and compare their roles in the differentiation of benign and malignant renal tumors. A number of investigations have compared the diagnostic value of IVIM or DKI over standard DWI for assessing renal tumors [16–21]. However, most of these studies have generally used small sample sizes. There are a growing number of studies using a hybrid IVIM-DKI model for tumor evaluation in recent years [22–25]. To our knowledge, no comparison of these different diffusion parameters in the discrimination of benign and malignant renal tumors in a large cohort has been investigated so far. The purpose of this study was to quantitatively compare the potential of various diffusion parameters obtained from DWI, IVIM, and DKI in the differentiation of benign and malignant renal tumors.

Materials and methods

Patients

Our institutional review board approved this study and waived the requirement to obtain informed consent. Between December 2014 and July 2018, 305 consecutive patients who were known to have, or were suspected of having renal tumors based on previous CT or ultrasonography examinations, underwent a preoperative MR imaging examination including both IVIM and DKI sequences in Zhongshan Hospital, Fudan University. The inclusion criteria were as follows: (a) primary renal lesions without prior treatment and (b) nephrectomy within 1 month after the MR imaging examination. Exclusion criteria included the following: (a) lesions without histopathological confirmation ($n = 52$), (b) lesions with antiangiogenic therapy ($n = 5$), (c) small renal tumors less than 1.0 cm in diameter ($n = 18$) or multiple lesions in one kidney ($n = 4$), and (d) MR images with severe susceptibility artifacts or respiratory motion artifacts ($n = 10$). Transitional cell carcinomas ($n = 14$), cystic renal tumors ($n = 4$), and renal cysts ($n = 8$) were also excluded, because the purpose of this study was to differentiate solid benign and malignant tumors originated from renal parenchyma. Ten cases of classical angiomyolipoma were excluded because they are very easy

to be differentiated from malignant renal tumors. The 1.0-cm lower threshold was selected to avoid potential confounding from partial volume averaging in smaller renal lesions. Finally, 125 patients were excluded, and a total of 180 patients (119 males and 61 females; mean age, 55.3 years; age range, 20–83 years) were included in the final cohort.

Pathological assessment revealed 166 cases of malignant renal tumors, which were divided into clear cell renal cell carcinoma (ccRCC) ($n = 124$) and non-ccRCC ($n = 42$) groups. The non-ccRCC malignant renal tumors were composed of papillary RCC ($n = 11$), chromophobe RCC ($n = 16$), clear cell papillary RCC ($n = 5$), MiT family translocation RCC ($n = 2$), non-Hodgkin lymphoma ($n = 2$), unclassified RCC ($n = 3$), and RCC with sarcomatous transformation ($n = 3$). Benign renal tumors ($n = 14$) included 12 fat poor angiomyolipomas and two renal oncocytomas. The mean interval between MR imaging and nephrectomy was 2.2 ± 2.5 days (range, 0–14 days).

Image data acquisition

All patients were examined with a 1.5-T MRI system (Magnetom Aera; Siemens Healthineers) equipped with an 18-channel body array coil. A routine multiparametric MR protocol included axial three-dimensional in- and out-of-phase T1-weighted interpolated breath-hold examination, T2-weighted turbo spin-echo pulse sequence with fat suppression, and pre- and postcontrast dynamic three-dimensional T1-weighted volumetric interpolated breath-hold examination at corticomedullary phase (20–25 s), nephrographic phase (80–90 s), and excretory phase (180 s) after injection of 0.1 mmol/kg gadopentetate dimeglumine (Magnevist; Bayer Schering Pharma AG) at a rate of 2 mL/s.

A multiple b value DWI scan was acquired using a work-in-progress echo-planar imaging sequence (WIP NO. 870) provided by the manufacturer (Siemens Healthineers). This WIP package supports a motion-insensitive PAT reference scan that is suitable for body diffusion measurements in free-breathing mode without respiratory gating in the acquisition. Parallel imaging was used, and fat was suppressed using spectral presaturation inversion recovery (SPIR). Eight b values (0, 25, 50, 80, 150, 300, 500, and 800 s/mm^2) were used, TR/TE 5100/70 ms; section thickness, 5 mm; gap, 1 mm; field of view, 380 mm × 308 mm; matrix, 128 × 128; scan time, 5 min 42 s. Then, DKI was acquired separately using a single-shot echo-planar imaging pulse sequence in free-breathing mode. Six b values that ranged from 0 to 2000 s/mm^2 (0, 200, 500, 1000, 1500, and 2000 s/mm^2) with three orthogonal directions for every b value. TR/TE was 7300/70 ms, section thickness, 5 mm; gap, 1 mm; 380 mm × 308 mm; and acquisition time, 2 min 32 s. Acquisition parameters of the axial multiple b value DWI and DKI sequences are listed in Table 1.

Table 1 Scanning parameters of diffusion sequences

Parameters	Multiple b value DWI	DKI
Repetition time (ms)	5100	7300
Echo time (ms)	70	70
Field of view (mm^2)	380 × 308	380 × 308
Voxel size (mm^3)	3.0 × 3.0 × 8.0	2.6 × 2.6 × 5.0
Scan matrix	128 × 128	128 × 128
Slice thickness (mm)	5	5
Gap (mm)	1	1
Directions	3	1
b values (s/mm^2)	0, 25, 50, 80, 150, 300, 500, 800	0, 200, 500, 1000, 1500, 2000
Averages	2, 2, 2, 3, 3, 3, 4, 4	2, 2, 3, 3, 4, 4
Scanning time	5 min 42 s	2 min 32 s

Image data analysis and processing

Multiple b value DWI data were used to compute mono- and biexponential models. Standard ADC map ($b = 0$ and 800 s/mm^2) was generated with the software integrated into the MR system (Syngo; Siemens Healthineers) according to the following equation: $S(b) = S0 \cdot \exp(-b \cdot ADC)$. IVIM parameter maps ($D$, D^*, f) were generated offline by using the postprocessing program provided with WIP NO.870 and fitting the following biexponential model [26]: $S(b)/S0 = (1-f) \cdot \exp(-bD) + f \cdot \exp[-b(D^* + D)]$, where $S(b)$ was the signal intensity at a given b value, $S0$ was the signal intensity for $b = 0$ s/mm^2, D was the diffusion parameter representing pure molecular diffusion, D^* was the pseudo-diffusion coefficient representing incoherent microcirculation within the voxel, and f was the perfusion fraction of the diffusion linked to microcirculation. DKI parameter maps (K and D) were calculated offline by using prototype software (Body Diffusion Toolbox; Siemens Healthineers). The software performed a voxel-by-voxel analysis and the six b value data were fitted to the following equation [27]: $S(b) = S0 \cdot \exp(-b \cdot D + b^2 \cdot D^2 \cdot K/6)$, where K is a unitless parameter that represents the deviation of water motion from Gaussian diffusion, and D is the corrected ADC without Gaussian bias. Least-squares fit was used for linear fitting with the monoexponential and DKI models, and IVIM data were fitted with the Levenberg-Marquardt nonlinear fitting algorithm.

ADC and IVIM parameters were evaluated on the Syngo workstation, while mean kurtosis (MK) and mean diffusivity (MD) were measured on the offline software (Body Diffusion Toolbox). Two observers (Y.Q.D, with 7 years of experience and J.J.Z, with 30 years of experience in urinary system imaging diagnosis) who were blinded to pathologic diagnosis analyzed in consensus all the parameter maps in conjunction with T1- and T2-weighted images. Free-hand regions of interest (ROIs) with a mean size of 14.99 ± 15.57 cm^2 (range from 0.93 to 104.10 cm^2) were outlined around the tumor on D and MD maps at three

representative slices and were simultaneously copied to D^*, f, ADC, and MK maps, respectively. In order to minimize the selection bias, the largest possible ROIs to include entire tumors were drawn. When the lesion showed isointense with surrounding renal parenchyma on the D or MD maps, the ROIs were selected by referring to T1- and T2-weighted images. These ROIs were selected on the basis of visual inspection of the parametric maps and the averaged values of the three slices were used for final analysis. Thirty cases were randomly selected from ccRCC, non-ccRCC, and benign renal tumor groups (10 cases in each group) and measured by two observers independently to assess the interobserver agreement of diffusion parameters.

Statistical analysis

Data were presented as mean ± standard deviation (SD). ADC, IVIM, and DKI parameters between malignant and benign renal tumor groups were compared using the Mann-Whitney U test or one-way ANOVA. Receiver operating characteristic (ROC) curve analysis was performed to evaluate the diagnostic performances and determine the optimal cutoff value of each parameter in predicting malignancy. Areas under the curves (AUCs) were compared using the DeLong method [28]. Interobserver agreement of diffusion parameter measurements was assessed by using the intraclass correlation coefficient (ICC) with 95% confidence interval (CI) ($\leqq 0.20$, slight; 0.21–0.40, fair; 0.41–0.60, moderate; 0.61–0.80, substantial; and 0.81–1.00, perfect) [29]. Statistical analyses were performed with SPSS (version 22.0) and MedCalc software (version 15.8.0). $p < 0.05$ was considered statistically significant.

Results

Population characteristics

A total of 124 patients (89 men and 35 women; mean age, 56.7 years; age range, 26–83 years) were confirmed with pathological examination to have ccRCCs (10 Fuhrman I, 92 Fuhrman II, 22 Fuhrman III, 0 Fuhrman IV). There were 42 patients (26 men and 16 women; mean age, 54.2 years; age range, 20–79 years) in the non-ccRCC group, and 14 patients (4 men and 10 women; mean age, 46.3 years; age range, 29–67 years) in the benign renal tumor group. The age of patients in benign renal tumor group was younger than those of the ccRCC group ($p = 0.013$). The average diameters of the ccRCC (4.7 ± 2.1 cm), non-ccRCC (4.6 ± 2.6 cm), and benign renal tumor (4.4 ± 2.7 cm) group were not statistically different ($p = 0.553$).

Diffusion metrics

Figures 1, 2, and 3 show the representative MR appearance on multiple diffusion images of pathologically confirmed

ccRCC, non-ccRCC, and benign renal tumor, respectively. ADC, IVIM, and DKI parameters of ccRCC, non-ccRCC, and benign renal tumors are shown in Fig. 4 and Table 2. The ADC, D, and MD values of ccRCCs were higher, while D^*, f, and MK values were lower than those of benign renal tumors (all $p < 0.025$). The D^* and f values of non-ccRCCs were lower than those of benign renal tumors ($p = 0.002$ and $p < 0.001$, respectively). However, the difference of ADC, D, MD, and MK values between non-ccRCCs and benign renal tumors was not statistically significant ($p > 0.05$). The ADC, D, MD, and f values of ccRCCs were higher, while MK values were lower than those of non-ccRCCs (all $p < 0.001$). However, the difference of D^* values between ccRCCs and non-ccRCCs was not statistically significant ($p = 0.127$). The agreements of diffusion parameters of the 30 randomly selected cases between two observers were perfect for ADC, D, MK, and MD with ICC (95%) of 0.974 (0.964–0.982), 0.976 (0.966–0.983), 0.904 (0.867–0.930), and 0.937 (0.913–0.955), respectively. The agreements of D^* and f were substantial between two observers with ICC (95%CI) of 0.785 (0.711–0.841) and 0.750 (0.666–0.815), respectively.

Diagnostic performance of multiple parameters

ROC curves of multiple diffusion parameters for predicting malignant renal tumors were plotted in Fig. 5, and the corresponding diagnostic test characteristics are shown in Table 3. The AUC values of ADC, D, D^*, f, MK, and MD were 0.849, 0.891, 0.708, 0.656, 0.862, and 0.838 for differentiating ccRCC from benign renal tumors, respectively. For pairwise comparisons of ROC curves, ADC was worse than D ($p = 0.048$) and not significantly different from D^* ($p = 0.170$), f ($p = 0.088$), MK ($p = 0.750$), and MD ($p = 0.811$). The difference in diagnostic efficacy among D, MK, and MD was not statistically significant (all $p > 0.05$). The AUC values of D^* and f were 0.772 and 0.866 for discrimination between non-ccRCC and benign renal tumors, respectively. For pairwise comparisons of ROC curves, the difference in diagnostic efficacy among D^* and f was not statistically significant ($p = 0.149$).

Discussion

In this study, we compared the diagnostic value of DWI, IVIM, and DKI in differentiating between benign and malignant renal tumors in a large cohort. Our results showed that DWI, IVIM, and DKI parameters were clinically feasible and of great value in differentiating between ccRCCs and benign renal tumors ($p < 0.025$). However, only IVIM parameters (D^* and f) were able to discriminate non-ccRCCs from benign renal tumors ($p < 0.01$).

The benign renal tumor group in our study was composed of fat poor angiomyolipoma ($n = 12$) and oncocytoma ($n = 2$),
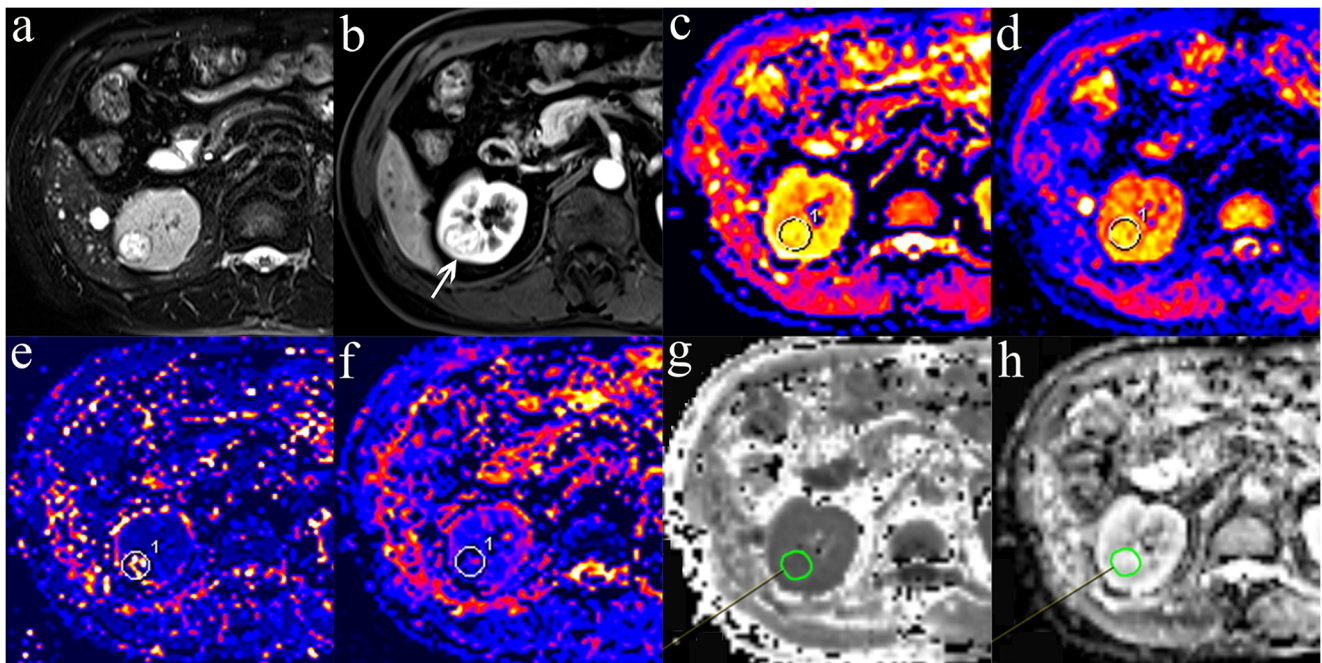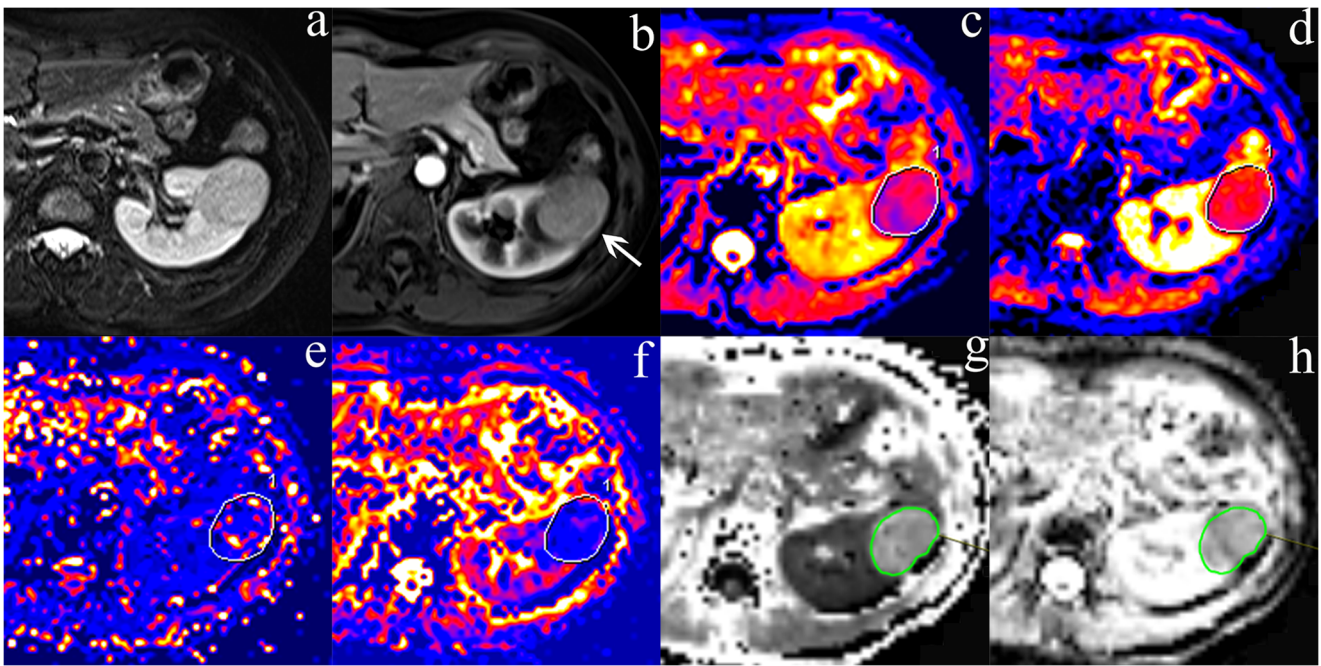
Fig. 1 A 67-year-old man with pathologically confirmed clear cell renal cell carcinoma in the right kidney. The lesion shows high signal intensity (SI) on T2-weighted image (**a**) and remarkable enhancement in corticomedullary phase (**b**). The lesion (ROI) demonstrates high SI on the ADC map (**c**), D map (**d**), D^* map (**e**), and mean diffusivity map (**h**) and low SI on the f map (**f**) and iso-SI on the mean kurtosis map (**g**), with values of 2.05×10^{-3} mm²/s, 1.73×10^{-3} mm²/s, 51.5×10^{-3} mm²/s, 2.78×10^{-3} mm²/s, 14.45%, and 0.60, respectively

which are the most common solid benign renal tumors misdiagnosed as renal cancer on preoperative imaging according to the surgical literature [2, 3, 5]. We found that ccRCCs had higher diffusion parameters (ADC, D, MD) than those of benign renal tumors (all $p < 0.025$). This might be partly explained by their histopathological characteristics. The alveolar and acinar structures of ccRCCs may dilate, producing microcystic and macrocystic patterns, so that the movement of water molecules is relatively unrestricted [30]. On the contrary, fat poor angiomyolipoma is composed of variable proportions of spindle cells or epithelioid smooth muscle cells and abnormal thick-walled blood vessels [30]. As a result, water molecules of fat poor angiomyolipoma in the extracellular interstitial space are obviously hindered because of higher cellularity and an increased viscosity of the tumor tissue [31]. Our findings are in line with previous studies [32–34]. The better accuracy of D values compared with ADC in differentiating ccRCCs from benign renal tumors in our study can be explained by the fact that ADC is a nonspecific measurement containing both the perfusion/microcirculation (f) and tissue cellularity (D) information [35], which may have opposite effects on the measurement of ADC in the evaluation of renal tumors, resulting in decreased sensitivity and specificity.

In our study, the perfusion-related IVIM parameters (D^* and f) showed greater diagnostic accuracy than those of ADC and DKI parameters in distinguishing non-ccRCCs from benign renal tumors. This is not difficult to understand,

since non-ccRCCs were mostly composed of renal tumors such as papillary RCC and chromophobe RCC with lesser enhancement than oncocytoma and fat poor angiomyolipoma in previous contrast-enhanced CT or MRI studies [36–38]. Previous study has reported a good correlation between f and perfusion-related parameters using gadolinium-based contrast agents for the discrimination of enhancing from non-enhancing renal lesions [35]. We noticed that D^* and f values of benign renal tumors were even higher than those of ccRCCs in our study ($p < 0.025$). This may partly be related to the fact that fat poor angiomyolipoma contains large and malformed blood vessels, whereas ccRCC has abundant capillaries [30]. Higher D^* values of fat poor angiomyolipoma in comparison with ccRCC have been reported in previous studies [19, 20], which is in agreement with our study. However, there is yet no consensus on the number of b values that should be used for extracting perfusion-sensitive information and the magnitude of b values that should be applied. Our study selected eight b values (0, 25, 50, 80, 150, 300, 500, and 800 s/mm²) according to the recommendations of Koh et al [39]. In a previous study [40], intraobserver reproducibility of renal tumors was excellent for ADC (coefficient of variation (CV), 3.45% to 3.82%; Bland-Altman limits of agreements (BA-LA), −14% to 18%) and D (CV, 3.65% to 4.3%; BA-LA, −14% to 16%), good for f (CV, 11.96% to 12.41%; BA-LA, −34% to 30%), and poor for D^* (CV, 25.0% to 33.65%; BA-LA, −111% to 101%). However, the agreements of diffusion parameters between two observers were perfect
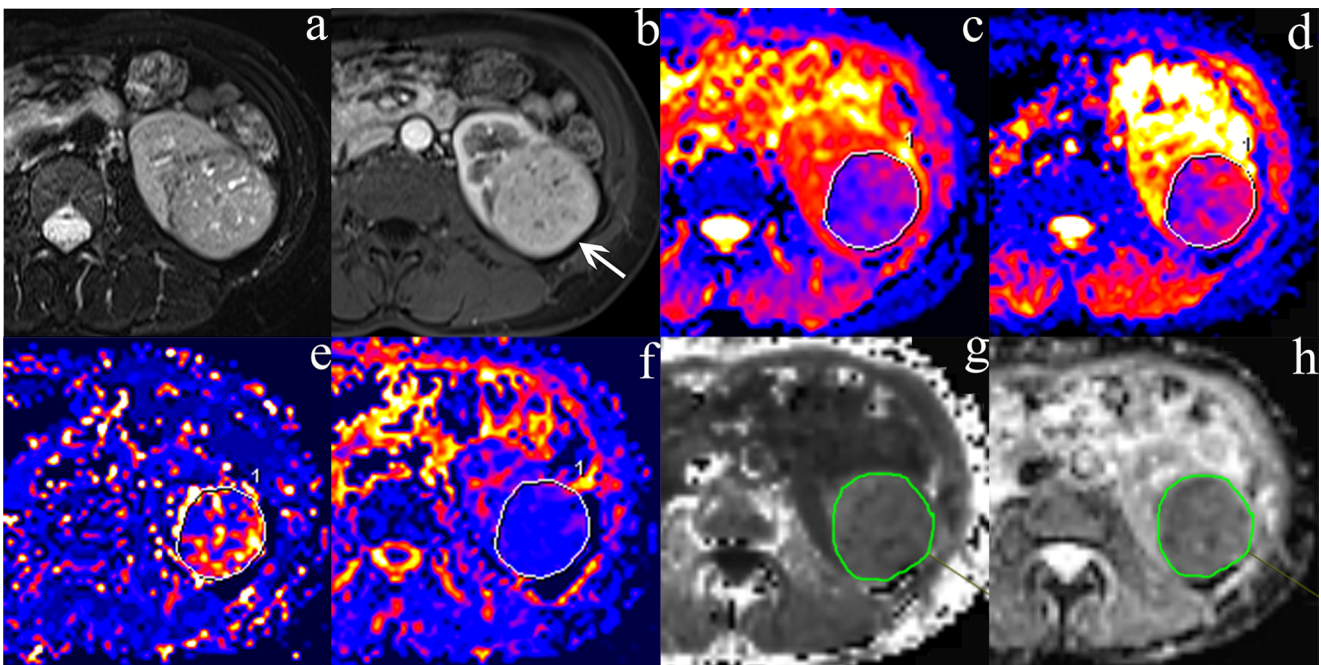
Fig. 2 A 65-year-old woman with pathologically confirmed chromophobe renal cell carcinoma in the left kidney. The lesion shows low signal intensity (SI) on T2-weighted image (**a**) and slight enhancement in corticomedullary phase (**b**). The lesion (ROI) demonstrates very low SI on the ADC map (**c**), D map (**d**), f map (**f**), and mean diffusivity map (**h**) and high SI on the D^* map (**e**) and mean kurtosis map (**g**), with values of 1.22×10^{-3} mm^2/s, 1.09×10^{-3} mm^2/s, 12.11%, 1.51×10^{-3} mm^2/s, 28.47×10^{-3} mm^2/s, and 0.93, respectively

for ADC and D and substantial for D^* and f in our study, with ICC (95%) of 0.974 (0.964–0.982), 0.976 (0.966–0.983), 0.785 (0.711–0.841), and 0.750 (0.666–0.815), respectively.

The possible reason might be that only the solid component of the tumor was included in previous study, while the entire tumor was included in our study. Although there were slight

Fig. 3 A 55-year-old woman with pathologically confirmed epithelioid angiomyolipoma in the left kidney. The lesion shows very low signal intensity (SI) on T2-weighted image (**a**) and moderate enhancement in corticomedullary phase (**b**). The lesion (ROI) demonstrates very low SI on the ADC map (**c**), D map (**d**), f map (**f**), and mean diffusivity map (**h**) and high SI on the D^* map (**e**) and mean kurtosis map (**g**), with values of 1.29×10^{-3} mm^2/s, 0.96×10^{-3} mm^2/s, 22.48%, 1.63×10^{-3} mm^2/s, 54.25×10^{-3} mm^2/s, and 0.87, respectively
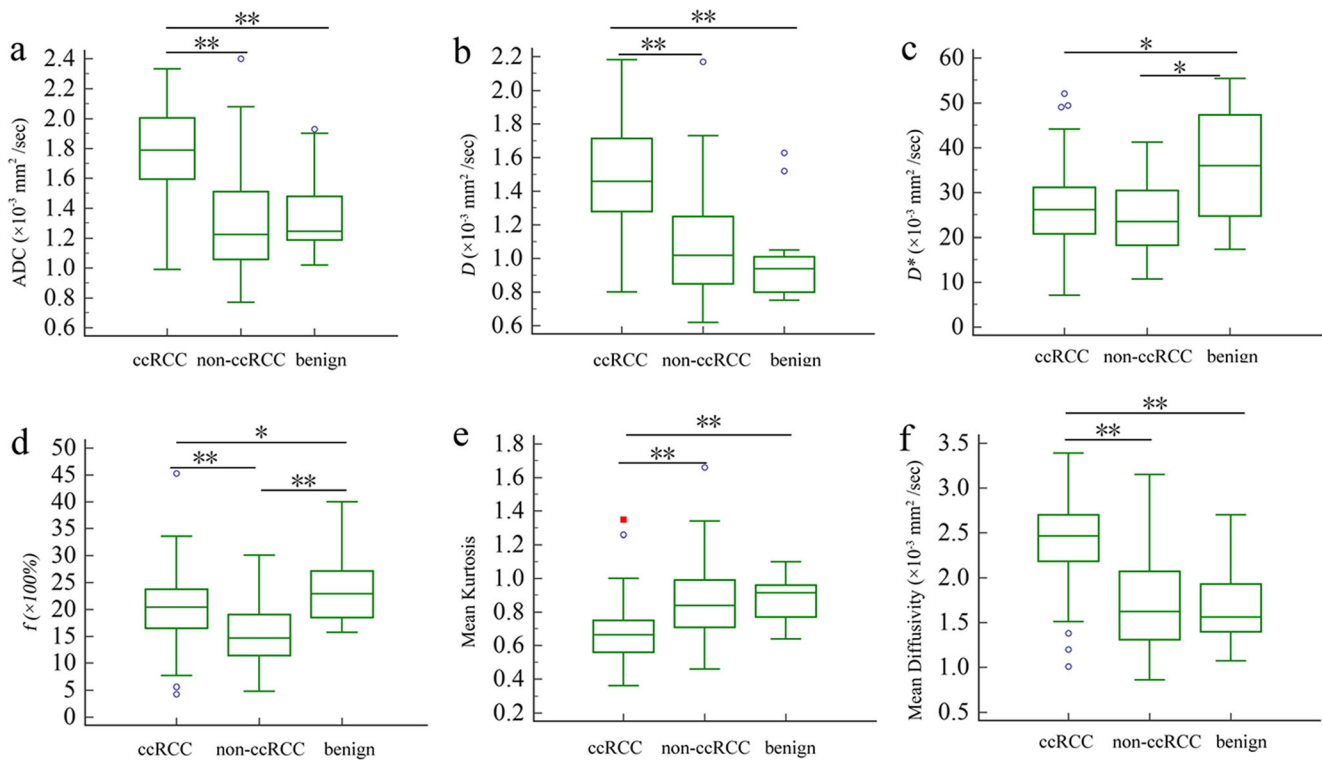
Fig. 4 Box-and-whisker plots show distributions of ADC (**a**), D (**b**), D* (**c**), f (**d**), mean kurtosis (**e**), and mean diffusivity (**f**) of ccRCC, non-ccRCC, and benign renal tumors. *p < 0.025, **p < 0.001. Dots mean outliers

differences in IVIM parameter values of renal tumors in previous literature, better diagnostic performance of IVIM over DWI has been reported in grading of ccRCCs [18], differentiating enhancing from non-enhancing renal tumors [35] and differentiating benign from malignant renal tumors, as well as RCC subtypes [16, 17, 20].

Non-Gaussian diffusion, which has the potential to extract more microstructural information beyond ADC, has been found to be useful in the differentiation between low-grade and high-grade ccRCCs [21]. Furthermore, negative correlations were found between MK and MD ($r = -0.56$, $p < 0.001$)

and between MD and nuclear-to-cytoplasm ratio ($r = -0.36$, $p < 0.005$), whereas MK and the nuclear-to-cytoplasm ratio were positively correlated ($r = 0.45$, $p = 0.003$) [21]. Unfortunately, no added value of the DKI parameters was found compared with ADC in differentiating malignant from benign renal tumors in our study. Theoretically, DKI model potentially better reflects water diffusivity in tissues at ultrahigh b values; it provides an additional parameter MK that contains specific information on the non-Gaussian diffusion behavior, and MD is presumed to be the more accurate measure of tissue diffusion, given its correction for non-Gaussian

Table 2 Diffusion parameters of malignant and benign renal tumors

Parameters	ccRCC	Non-ccRCC	Benign	p value		
				ccRCC vs benign	Non-ccRCC vs benign	ccRCC vs non-ccRCC
ADC	1.78 ± 0.29	1.31 ± 0.34	1.35 ± 0.29	< 0.001*	0.690*	< 0.001*
D	1.48 ± 0.30	1.09 ± 0.32	0.99 ± 0.26	< 0.001	0.205	< 0.001
D*	26.51 ± 8.53	24.26 ± 8.02	35.83 ± 12.26	0.011	0.002	0.127
f	20.17 ± 5.79	15.22 ± 5.30	24.25 ± 7.14	0.013*	< 0.001*	< 0.001*
MK	0.68 ± 0.15	0.88 ± 0.24	0.89 ± 0.14	< 0.001	0.596	< 0.001
MD	2.43 ± 0.45	1.74 ± 0.57	1.73 ± 0.51	< 0.001	0.910	< 0.001

ADC apparent diffusion coefficient, *D* true diffusivity, *D** pseudo-diffusion coefficient, *f* perfusion fraction, *MK* mean kurtosis, *MD* mean diffusivity. Data are presented as mean ± standard deviation.*Diffusion parameters were compared by using one-way ANOVA, otherwise were compared using the Mann-Whitney *U* test. The *p* values in italics are of statistical significance. ADC, *D*, *D**, and MD values are presented in $\times 10^{-3}$ mm^2/s, *f* is presented in percentage, MK is unitless

Fig. 5 Receiver operating characteristic curves of the diagnostic performance of ADC, D, D^*, f, mean kurtosis, and mean diffusivity for differentiating between ccRCC and benign renal tumors (**a**) as well as D^* and f for differentiating between non-ccRCC and benign renal tumors (**b**). Numbers are areas under the curves
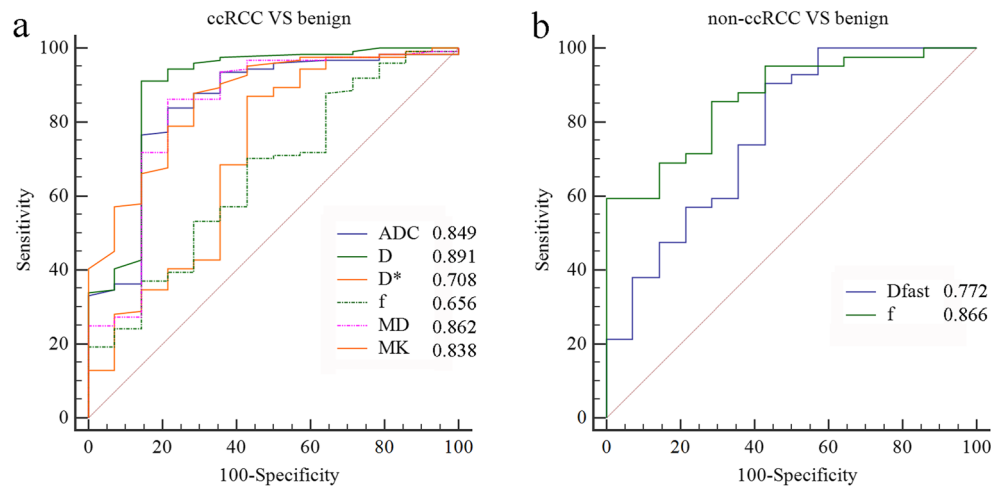
diffusion behavior [15]. However, obtaining sufficient signal-to-noise ratio at high b values in order for the calculated DKI metrics to be accurate is particularly challenging in body imaging. Rosenkrantz et al [14] suggested that at least three b values and three directions are needed for the application of the DKI sequence. We selected b values of 0, 200, 500, 1000, 1500, and 2000 s/mm^2 and three diffusion directions to reduce potential perfusion effects when b value is less than 200 s/mm^2 in our study [14]. The agreements of MK and MD between two observers were perfect in our study, with ICC (95%) of 0.904 (0.867–0.930) and 0.937 (0.913–0.955), respectively. Although most of the published papers consider that DKI is superior to DWI in tumor diagnosis and prognosis evaluation, no added values of DKI over DWI have also been reported by Li et al [41] in ovarian tumors, Roethke et al [42] and Tamura et al [43] in prostate cancer, Wan Q et al [24] and Das et al [44] in pulmonary nodules, and Yang L et al [45] in liver fibrosis. The controversial results have implications for ongoing efforts to optimize clinical DKI protocols, and large-

scale prospective studies are undoubtedly needed to further validate our findings of DKI in renal tumors.

This study had several limitations. First, due to the limited number of non-ccRCCs and benign tumors of each histologic subtype, we simply divided renal tumors into three groups (ccRCCs, non-ccRCCs, and benign renal neoplasms). In reality, some histologic subtypes within those broad classes have different combinations of microvascular/microstructural features which may limit their distinction as an amalgamated class. Second, the regions of interest were selected in three representative slices instead of the entire renal tumors in this study, which might lead to some selection bias owing to tumor heterogeneity. Third, other advanced DW imaging models were not evaluated, and histogram metrics of the entire tumor were not assessed. In the future, the combination of different diffusion models with the detailed histologic subtypes should be investigated further in a larger study.

In conclusion, our results suggest that the D value is the best parameter for differentiating ccRCC from benign renal

Table 3 Diagnostic test characteristics of diffusion parameters in differentiating malignant from benign renal tumors

Parameters	AUC (95% CI)	Cutoff value	Sensitivity	Specificity	Accuracy
ccRCC ($n = 124$) vs benign ($n = 14$)					
ADC	0.849 (0.778–0.904)	> 1.48	83.87% (104/124)	78.57% (11/14)	83.33% (115/138)
D	0.891 (0.827–0.938)	> 1.05	91.13% (113/124)	85.71% (12/14)	90.58% (125/138)
D^*	0.708 (0.624–0.782)	≤ 34.50	87.10% (108/124)	57.14% (8/14)	84.06% (116/138)
f	0.656 (0.570–0.735)	≤ 22.65	70.16% (87/124)	57.14% (8/14)	68.84% (95/138)
MK	0.862 (0.793–0.915)	≤ 0.84	87.90% (109/124)	71.43% (10/14)	86.23% (119/138)
MD	0.838 (0.765–0.895)	> 1.93	86.29% (107/124)	78.57% (11/14)	85.51% (118/138)
Non-ccRCC ($n = 42$) vs benign ($n = 14$)					
D^*	0.772 (0.641–0.874)	≤ 33.91	90.48% (38/42)	57.14% (8/14)	82.14% (46/56)
f	0.866 (0.748–0.942)	≤ 15.51	59.52% (25/42)	100.00% (14/14)	69.64% (39/56)

ADC apparent diffusion coefficient, *D* true diffusivity, *D** pseudo-diffusion coefficient, *f* perfusion fraction, *MK* mean kurtosis, *MD* mean diffusivity, *AUC* area under ROC curve, *95% CI* 95% confidence interval. Cutoff values of ADC, D, D*, and MD are presented in × 10^{-3} mm^2/s, *f* is presented in percentage, MK is unitless

tumors, and the *f* value is the best parameter for differentiating non-ccRCC from benign renal tumors. However, our observations do not show clear added value for DKI compared with conventional DWI for discrimination between malignant and benign renal tumors.

Compliance with ethical standards

Guarantor The scientific guarantor of this publication is Jianjun Zhou.

Conflict of interest The authors of this manuscript declare no relationships with any companies, whose products or services may be related to the subject matter of the article.

Statistics and biometry No complex statistical methods were necessary for this paper.

Informed consent Written informed consent was waived by the Institutional Review Board.

Ethical approval Institutional Review Board approval was obtained.

Methodology
• retrospective
• cross-sectional study/diagnostic study
• performed at one institution

References

1. Hollingsworth JM, Miller DC, Daignault S, Hollenbeck BK (2006) Rising incidence of small renal masses: a need to reassess treatment effect. J Natl Cancer Inst 98:1331–1334

2. Kutikov A, Fossett LK, Ramchandani P et al (2006) Incidence of benign pathologic findings at partial nephrectomy for solitary renal mass presumed to be renal cell carcinoma on preoperative imaging. Urology 68:737–740

3. Fujii Y, Komai Y, Saito K et al (2008) Incidence of benign pathologic lesions at partial nephrectomy for presumed RCC renal masses: Japanese dual-center experience with 176 consecutive patients. Urology 72:598–602

4. Lee SH, Park SU, Rha KH et al (2010) Trends in the incidence of benign pathological lesions at partial nephrectomy for presumed renal cell carcinoma in renal masses on preoperative computed tomography imaging: a single institute experience with 290 consecutive patients. Int J Urol 17:512–516

5. Bauman TM, Potretzke AM, Wright AJ, Knight BA, Vetter JM, Figenshau RS (2017) Partial nephrectomy for presumed renal-cell carcinoma: incidence, predictors, and perioperative outcomes of benign lesions. J Endourol 31:412–417

6. Forbes CM, Rendon RA, Finelli A et al (2016) Disease progression and kidney function after partial vs. radical nephrectomy for T1 renal cancer. Urol Oncol 34:417–486

7. Jewett MA, Mattar K, Basiuk J et al (2011) Active surveillance of small renal masses: progression patterns of early stage kidney cancer. Eur Urol 60:39–44

8. Malayeri AA, El KR, Zaheer A et al (2011) Principles and applications of diffusion-weighted imaging in cancer detection, staging, and treatment follow-up. Radiographics 31:1773–1791

9. Ye J, Kumar BS, Li XB, Li HM, Zhou YW, Liu LQ (2017) Clinical applications of diffusion-weighted magnetic resonance imaging in diagnosis of renal lesions - a systematic review. Clin Physiol Funct Imaging 37:459–473

10. Li Y, Wang Y, Qin J, Wu J, Dai X, Xu J (2018) Meta-analysis of diffusion-weighted imaging in the differential diagnosis of renal lesions. Clin Imaging 52:264–272

11. Le Bihan D, Turner R (1992) The capillary network: a link between IVIM and classical perfusion. Magn Reson Med 27:171–178

12. Zhang JL, Sigmund EE, Chandarana H et al (2010) Variability of renal apparent diffusion coefficients: limitations of the monoexponential model for diffusion quantification. Radiology 254:783–792

13. Le Bihan D, Breton E, Lallemand D, Grenier P, Cabanis E, Laval-Jeantet M (1986) MR imaging of intravoxel incoherent motions: application to diffusion and perfusion in neurologic disorders. Radiology 161:401–407

14. Rosenkrantz AB, Padhani AR, Chenevert TL et al (2015) Body diffusion kurtosis imaging: basic principles, applications, and considerations for clinical practice. J Magn Reson Imaging 42:1190–1202

15. Jensen JH, Helpern JA, Ramani A, Lu H, Kaczynski K (2005) Diffusional kurtosis imaging: the quantification of non-Gaussian water diffusion by means of magnetic resonance imaging. Magn Reson Med 53:1432–1440

16. Chandarana H, Kang SK, Wong S et al (2012) Diffusion-weighted intravoxel incoherent motion imaging of renal tumors with histopathologic correlation. Invest Radiol 47:688–696

17. Gaing B, Sigmund EE, Huang WC et al (2015) Subtype differentiation of renal tumors using voxel-based histogram analysis of intravoxel incoherent motion parameters. Invest Radiol 50:144–152

18. Shen L, Zhou L, Liu X, Yang X (2017) Comparison of biexponential and monoexponential DWI in evaluation of Fuhrman grading of clear cell renal cell carcinoma. Diagn Interv Radiol 23:100–105

19. Zhu Q, Zhu W, Ye J, Wu J, Chen W, Hao Z (2019) Value of intravoxel incoherent motion for differential diagnosis of renal tumors. Acta Radiol 60:382–387

20. Ding Y, Zeng M, Rao S, Chen C, Fu C, Zhou J (2016) Comparison of biexponential and monoexponential model of diffusion-weighted imaging for distinguishing between common renal cell carcinoma and fat poor angiomyolipoma. Korean J Radiol 17:853–863

21. Dai Y, Yao Q, Wu G et al (2016) Characterization of clear cell renal cell carcinoma with diffusion kurtosis imaging: correlation between diffusion kurtosis parameters and tumor cellularity. NMR Biomed 29:873–881

22. Iima M, Kataoka M, Kanao S et al (2018) Intravoxel incoherent motion and quantitative non-Gaussian diffusion MR imaging: evaluation of the diagnostic and prognostic value of several markers of malignant and benign breast lesions. Radiology 287:432–441

23. Xiao Z, Zhong Y, Tang Z et al (2018) Standard diffusion-weighted, diffusion kurtosis and intravoxel incoherent motion MR imaging of sinonasal malignancies: correlations with Ki-67 proliferation status. Eur Radiol 28:2923–2933

24. Wan Q, Deng YS, Lei Q et al (2019) Differentiating between malignant and benign solid solitary pulmonary lesions: are intravoxel incoherent motion and diffusion kurtosis imaging superior to conventional diffusion-weighted imaging? Eur Radiol 29:1607–1615

25. Lu Y, Jansen JF, Mazaheri Y, Stambuk HE, Koutcher JA, Shukla-Dave A (2012) Extension of the intravoxel incoherent motion

model to non-Gaussian diffusion in head and neck cancer. J Magn Reson Imaging 36:1088–1096

26. Luciani A, Vignaud A, Cavet M et al (2008) Liver cirrhosis: intravoxel incoherent motion MR imaging–pilot study. Radiology 249:891–899

27. Wang WT, Yang L, Yang ZX et al (2018) Assessment of microvascular invasion of hepatocellular carcinoma with diffusion kurtosis imaging. Radiology 286:571–580

28. DeLong ER, DeLong DM, Clarke-Pearson DL (1988) Comparing the areas under two or more correlated receiver operating characteristic curves: a nonparametric approach. Biometrics 44:837–845

29. Landis JR, Koch GG (1977) The measurement of observer agreement for categorical data. Biometrics 33:159–174

30. Moch H, Humphrey PA, Ulbright TM, Reuter VE (2016) WHO classification of tumours of the urinary system and male genital organs, 4th edn. IARC, Lyon

31. Squillaci E, Manenti G, Cova M et al (2004) Correlation of diffusion-weighted MR imaging with cellularity of renal tumours. Anticancer Res 24:4175–4179

32. Tanaka H, Yoshida S, Fujii Y et al (2011) Diffusion-weighted magnetic resonance imaging in the differentiation of angiomyolipoma with minimal fat from clear cell renal cell carcinoma. Int J Urol 18: 727–730

33. Agnello F, Roy C, Bazille G et al (2013) Small solid renal masses: characterization by diffusion-weighted MRI at 3 T. Clin Radiol 68: e301–e308

34. Sasamori H, Saiki M, Suyama J, Ohgiya Y, Hirose M, Gokan T (2014) Utility of apparent diffusion coefficients in the evaluation of solid renal tumors at 3T. Magn Reson Med Sci 13:89–95

35. Chandarana H, Lee VS, Hecht E, Taouli B, Sigmund EE (2011) Comparison of biexponential and monoexponential model of diffusion weighted imaging in evaluation of renal lesions: preliminary experience. Invest Radiol 46:285–291

36. Zhang J, Lefkowitz RA, Ishill NM et al (2007) Solid renal cortical tumors: differentiation with CT. Radiology 244:494–504

37. Sasiwimonphan K, Takahashi N, Leibovich BC, Carter RE, Atwell TD, Kawashima A (2012) Small (<4 cm) renal mass: differentiation of angiomyolipoma without visible fat from renal cell carcinoma utilizing MR imaging. Radiology 263:160–168

38. Vargas HA, Chaim J, Lefkowitz RA et al (2012) Renal cortical tumors: use of multiphasic contrast-enhanced MR imaging to differentiate benign and malignant histologic subtypes. Radiology 264:779–788

39. Koh DM, Collins DJ, Orton MR (2011) Intravoxel incoherent motion in body diffusion-weighted MRI: reality and challenges. AJR Am J Roentgenol 196:1351–1361

40. Pan J, Zhang H, Man F et al (2018) Measurement and scan reproducibility of parameters of intravoxel incoherent motion in renal tumor and normal renal parenchyma: a preliminary research at 3.0 T MR. Abdom Radiol (NY) 43:1739–1748

41. Li HM, Zhao SH, Qiang JW et al (2017) Diffusion kurtosis imaging for differentiating borderline from malignant epithelial ovarian tumors: a correlation with Ki-67 expression. J Magn Reson Imaging 46:1499–1506

42. Roethke MC, Kuder TA, Kuru TH et al (2015) Evaluation of diffusion kurtosis imaging versus standard diffusion imaging for detection and grading of peripheral zone prostate cancer. Invest Radiol 50:483–489

43. Tamura C, Shinmoto H, Soga S et al (2014) Diffusion kurtosis imaging study of prostate cancer: preliminary findings. J Magn Reson Imaging 40:723–729

44. Das SK, Yang DJ, Wang JL, Zhang C, Yang HF (2017) Non-Gaussian diffusion imaging for malignant and benign pulmonary nodule differentiation: a preliminary study. Acta Radiol 58:19–26

45. Yang L, Rao S, Wang W et al (2018) Staging liver fibrosis with DWI: is there an added value for diffusion kurtosis imaging? Eur Radiol 28:3041–3049